

P, S, and K as Tracers of Aqueous Processing on Ryugu

G. J. Flynn¹, and P. Northrup²

¹*SUNY-Plattsburgh, 101 Broad St., Plattsburgh, NY 12901 (flynnji@plattsburgh.edu)*

²*Stony Brook University, Department of Geosciences (paul.northrup@stonybrook.edu)*

JAXA's Hayabusa2 spacecraft delivered ~5.4 g of material from asteroid 162173 Ryugu. Nakamura et al. [1], who analyzed seven samples from the first collection site, indicated the major lithology was dominated by phyllosilicates, with carbonates, Fe-sulfides, Fe-oxides, and Fe-bearing hydroxyapatite. We were loaned five polished sections prepared from 3 to 5 mm size fragments from the first collection site – A0026-01, A0026-02, A0055-1, A0055-2, and A0055-3. These samples were studied previously. Tack et al. [2] measured REEs in A0055, before it was sectioned, and found REEs were mainly enriched in some Ca- and Sr-rich phases they suggested were apatite. Nakamura et al. [1] found CI-like bulk element abundance in 17 samples including A0026 and A0055. Gainsforth et al. [3] examined a FIB section from A0026. Mikouchi et al. [4] analyzed polished sections of both A0055 and A0026. The abundant phyllosilicates [1] demonstrate there was significant hydrothermal processing of these Ryugu samples. Likely products of this alteration are phosphates, carbonates, and sulfates whose abundances and compositions can characterize the fluids responsible for the alteration. To study these minerals, we used synchrotron x-ray fluorescence (XRF) to map element distributions and x-ray absorption spectroscopy (XAS) to characterize the minerals in the five sections. We focused on P, S, and K, which are sensitive indicators of aqueous mobilization.

P-mapping: Synchrotron XRF element mapping of the three A0055 sections clearly show two distinct P-lithologies (Fig. 1), with about half of each section having numerous, relatively large P-rich grains while the other half has smaller P-rich grains. The mean P/Si ratio in each lithology of the A0055 sections is quite consistent, with P/Si about 0.04 to 0.05 in the high-P areas and an order-of-magnitude lower, ~0.005, in the low-P lithology. The two A0026 samples have a more uniform distribution of P-rich grains which are smaller than the grains in the high-P lithology of the A0055 samples, but more numerous than those in the A0055 low-P lithology. The P/Si ratio in the A0026 sections is ~0.025, distinct from the high- and low-P lithologies in A0055, suggesting these Ryugu samples experienced at least three distinct degrees of hydrothermal processing.

Mikouchi et al. [3] characterized the same dry polished [1] A0055-1 section that we examined, determining the degree of aqueous processing based on the abundance and types of carbonate. In A0055-1 they found no olivine bearing clasts, present in their Lithologies I and II, which show the lowest aqueous processing. They identified three lithologies in A0055-1 based on carbonates: Lithology III dolomite-bearing; Lithology V carbonate aggregates; and Lithology VI carbonate-poor (<1 vol.%). Our XRF maps of A0055-1 show very low P in their Lithology VI areas, with P/Si ranging from 0.0048 to 0.0082. This suggests the carbonate-poor regions experienced very little deposition of P from the fluid that produced phyllosilicates. However, the low-P and high-P regions in A0055-1 both overlap their carbonate Lithology III. Our Ca-XAS and Mn-XAS of carbonates in these samples identified Mn-bearing dolomite as the dominant carbonate (Fig. 2).

Apatite: The apatite structure accepts a wide range of elements, so it is a good indicator of fluid composition. Since apatite accepts F, Cl, or OH in the anion position, the proportions of F, Cl and OH in apatite reflect the halogen and water content of the fluid. Gainsforth et al. [3] identified one apatite grain in an A0026 FIB section and found a Mn-poor core with a Mn-rich zone on the surface enriched in Fe, F, and Na compared to the core. This suggests alteration by two different fluids.

All Ca-apatite grains have distinctive P-XAS, with a peak at ~2152 eV and a shoulder on the high-energy side. The energy of this shoulder peak shifts progressively lower in energy as the apatite composition varies from fluorapatite to hydroxyapatite to chlorapatite. Most P hot-spots in these five sections have P-XAS spectra consistent with apatite (Fig. 3), which is believed to be a hydrothermal alteration phase. The small difference in position of the shoulder at ~2156 eV in the Ryugu apatite spots, compared to the fluorapatite standard (top spectrum in Fig. 3), indicates the Ryugu apatite has significant hydroxy- and/or chlorapatite components. Some of the Ryugu apatite grains showed Cl spatially coincident with the apatite in the XRF maps. To address the question of Cl in the apatite we performed Cl-XAS, which demonstrated that the Cl was not in the apatite crystals. (Cl is present in high abundance in the epoxy mounts.) The absence of significant chlorapatite combined with the XAS spectral shift from fluorapatite indicates a significant hydroxyapatite component in the Ryugu samples. The quantitative F:OH:Cl ratio in individual apatite crystals will be determined in the planned electron microprobe analyses.

A particle-size effect on the XAS has been described in apatite XAS by Szerlag (in press). The peak height is lower in more crystalline spots due to electronic interactions across larger crystalline domains. We see significant variations in peak heights in different spots in both A0026 and A0055 that have the same P count rate, indicating that some spots are nanocrystalline aggregates or highly disordered while other spots are larger, well crystalline apatite. Seifert et al. [5], using cathodoluminescence, observed similar results in Bennu samples. They reported complex luminescence zoning in some anhedral apatite grains that range in size from about 5 to 12 μm in a Bennu sample. Our planned electron microprobe analyses should reveal if the individual apatite grains in these aggregates differ in composition, suggesting they formed from fluids of different compositions.

Although most of the P hot-spots were identified as apatite by XAS, there were two types of exceptions. A few phosphates showed no shoulder on the high energy side of the pre-edge peak (e.g., Fig. 3, bottom spectrum). Electron microprobe characterization of these phosphate spots may allow identification of this phase. In addition, we found rare, small phosphides in the matrix. The large difference in the pre-edge peaks between phosphide and phosphate in P-XAS allowed functional group specific mapping of phosphide and phosphate. Both A0055 and A0026 had regions where phosphide and phosphate were both identified (Fig. 4). However, we did not see phosphate rims surrounding phosphide cores as would be expected if an initial phosphide were attacked and incompletely altered by the fluid. Mikouchi et al. [4] identified Fe,Ni phosphide associated with

olivine [3] in grains from the second collection site. However, we found rare, small phosphides in these A0026 and A0055 sections (Fig. 3), indicating incomplete alteration of phosphide, even where Mikouchi et al. found no olivine [3].

Sulfide/Sulfate: Alteration of sulfide to sulfate has been reported in CM chondrites [6]. Sulfate is easily distinguished from sulfide because of the large energy difference in S-XAS. Sulfate is characterized by a peak at ~2483 eV, as illustrated by the bottom spectrum in Fig. 5, which also shows a sulfate standard. The upper set of spectra show 3 spots on A0026-02, all matching pyrrhotite with no sulfate, while the lower set are 4 spots on A0055-1 that also match pyrrhotite but with some sulfate within the 5- μm beam spot size. The sulfate in the A0055 sections suggests significant interaction with an oxidizing fluid. If all the sulfide grains experienced the same degree of aqueous processing, resulting in the same depth of alteration, we would expect the S hot-spots to show an anti-correlation between sulfate/sulfide ratio and size. We see no evidence for this correlation, suggesting different regions of these samples experienced different degrees of hydrothermal processing. The S/Si ratio ranges from 0.38 to 0.56, bracketing the CI ratio, in these Ryugu samples.

We identified grains of sulfide surrounding silicates (Fig. 6, left). These features may be similar to the inclusions identified in Bennu samples and Tagish Lake by Smith et al. [7]. These inclusions were described as being from 2 to 15 micrometers in size with a mostly homogeneous interior consisting primarily of fine-grained Mg-rich phyllosilicates with a rim of hexagonal sulfides. They suggested that these clasts likely formed under reducing conditions, possibly enstatite chondrite material exogenous to Bennu. We also identified circular rims of phosphate surrounding silicates, which need further study, in these Ryugu samples.

K-distribution: We mapped the K distribution, and found K to be heterogeneously distributed, but spatially coincident with the phyllosilicates. However, the low-K and high-K regions in A0055-1 (Fig. 6, right) do not correlate with any of the lithologies from Mikouchi et al. [4] or with the low-P and high-P lithologies we identified (Fig. 1). It is not clear whether this heterogeneous K distribution resulted from uneven distribution of the fluid or subsequent K leaching by the fluid.

Taken together, these results suggest the Ryugu parent body experienced multiple episodes of hydrothermal processing by fluids of different compositions. Further characterization of these Ryugu samples is in progress.

References: [1] Nakamura, T. et al. (2023) Science 379, eabn671. [2] Tack et al. (2022) Earth, Planets, Space 74, #146. [3] Gainsforth, Z. et al. (2024) Meteoritics and Planetary Science, doi: 10.1111/maps.14161. [4] Mikouchi et al. (2022) <https://curation.isas.jaxa.jp/symposium/abstract/2022/S22-01>. [5] Seifert et al. (2024) MetSoc, Abstract #6208. [6] Airieau et al. (2005) GCA, 69, 4166–4171. [7] Smith et al. (2024) MetSoc Abstract #6075.

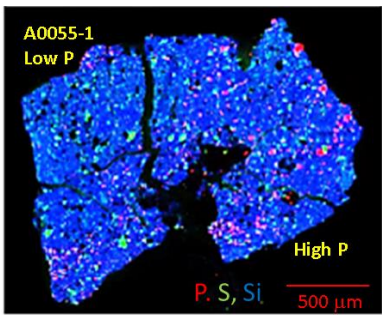


Figure 1: P, S, Si 3-color XRF map of A0055-1.

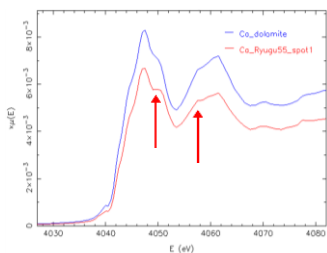


Figure 2 Ca-XAS of a large carbonate grain in A0055-1. The features that distinguish the bilayered carbonate (dolomite) from monolayered carbonates calcite or Ca-bearing magnesite are indicated by the arrows.

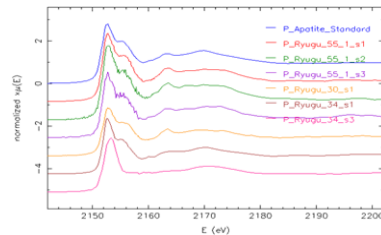


Figure 3: P-XAS of fluorapatite (top), and Ryugu P hot-spots. The bottom spectrum shows a phosphate with no shoulder on the peak.

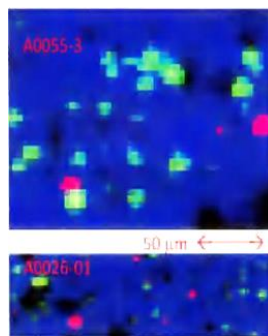


Figure 4: Phosphide (red) and phosphate (green) in A0055-3 and A0026-01.

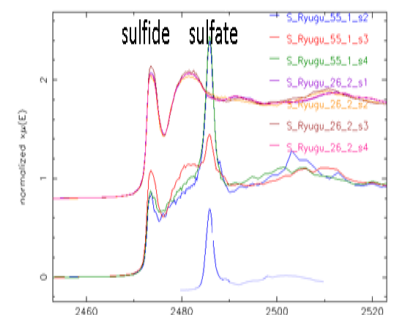


Figure 5: S-XAS of A0026-02 (top three spectra) showing only sulfide, and S-XAS of A0055-1 (next four spectra) showing sulfate as well as sulfide.

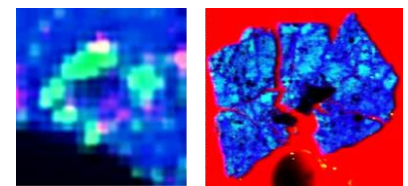


Figure 6: (Left) Three color image showing the sulfide grains (green) forming a rim around a silicate region of A0026-01. (Right) Cl (red), K (green), Si (blue) 3-color map (K shown in light blue) of A0055-1. (Cl in epoxy.)